A New Adaptive Terminal Sliding Mode Speed Control in Flux Weakening Region for DTC Controlled Induction Motor Drive

Barış Çavuş and Mustafa Aktaş

***Abstract*—Running over the motor rated speed is crucial in applications, such as electric vehicles. The flux weakening technique for reaching high speed used in this article is model predictive control (MPC) based control. The method ensures that the induction motor operates far above its normal speed, however, there are significant issues, such as ripple in terms of speed, torque, flux, etc. A novel sliding mode control (SMC) is suggested in this article to both improve induction motor control performance and get rid of the drawbacks of MPC-based flux control. The study findings revealed that the chattering problem has been solved significantly as well as improving the speed and torque control performance. By including the exponential and constant rate elements, new SMC technique has been developed to address the chattering issue. The time to reach the steady state in speed is decreased using the suggested adaptive terminal SMC technique, and the chattering issue is resolved. The simulation and experimental results show that the suggested adaptive terminal SMC approach reduced ripple and chattering issues while improving other factors like error reduction and time to steady state in speed. In addition to enhancing the motor control performance, less total harmonic distorsionof the motor current, flux, and torque ripple are achieved.**

***Index Terms*—Adaptive terminal sliding mode control (SMC), direct torque control (DTC), flux weakening, induction motor, model predictive control (MPC).**

I. Introduction

HIGH efficiency, good dynamic speed, dynamic responsiveness, and reliability are required from electric vehicles [1]. High performance is among the most important concerns of motor for low speed and torque especially when driving in cities. Induction motors are frequently utilized in electric vehicles as a result. [2], [3].

Uncontrollable driving of induction motors can lead to problems like high current level, low dynamic reaction, and high error in motor values (torque, speed, and flux). To get rid of the drawbacks, modern control techniques like vector control should be applied. Direct torque control (DTC), which performs well in alternative current motor applications, is utilized in this article [4], [5]. In 1985, Takahashi and Noguchi proposed DTC [6]. The benefit of this approach, unlike field oriented control (FOC) is that DTC reacts to changes in speed and torque very fast. Other benefits include little dependence on motor parameters and the absence of axis transformation [7]. Axis conversion is not necessary; therefore, processing proceeds quickly. The output ripple is the main drawback of this method [8].

It's essential to run the motor at a speed higher than its nominal speed, particularly for specific applications like electric vehicles [9]. The induction motor control must be carried out by fulfilling three conditions in flux weakening region. These three requirements include little change in motor characteristics [10], [11], accurate monitoring of motor references [12], and minimal reference voltage ripple [9]. Examining the studies in the flux weakening control reveals that they may be divided into four categories: classical flux weakening inversely proportional to speed ($1/\omega_r$) [13], [14], [15], voltage closed loop PI controller [16], [17], [18], look-up tables [19], [20], and model predictive techniques [9], [21], [22]. One of these techniques, model predictive control (MPC), is highly effective since it depends less on changes in system parameters and, like other strategies, takes into account both the present state and its potential future states of system [23], [24], [25]. MPC is therefore less likely than other control techniques to result in steady-state error. There are very few studies on MPC-based flux weakening control for DTC controlled motor driver, and it has been found that flux and torque ripple are very high [26]. The MPC-based flux weakening method was mostly employed in the studies for current control in FOC controlled motor drive [27], [28], [29].

Numerous linear speed control methods have been suggested to govern systems in the literature. A widespread linear control technique is proportional-integral (PI) control. [30]. For the regulation of systems with nonlinear and time-varying parameters, such as induction motors, linear control approaches perform inadequately. This is due to the fact that variables like resistance and time constants alter with time and have an impact on the load. Linear control methods, such as the PI control method cannot keep up with these changes [31], [32]. The performance of the straightforward PI control for controlling motor speed is adversely impacted by disturbance effects and parameter changes. This causes errors and ripples in motor speed. Errors and ripples that will occur in speed and torque for motor used in

Manuscript received 26 April 2023; revised 14 August 2023; accepted 17 October 2023. Date of publication 23 October 2023; date of current version 6 December 2023. This work was supported by TÜBİTAK under Grant 123E001. Recommended for publication by Associate Editor H. Hofmann. *(Corresponding author: Barış Çavuş.)*

The authors are with the Electrical and Electronics Engineering, Ondokuz Mayis University, Atakum, Samsun, Türkiye (e-mail: baris.cavus@omu.edu.tr; mustafa.aktas@omu.edu.tr).

Color versions of one or more figures in this article are available at https://doi.org/10.1109/TPEL.2023.3326383.

Digital Object Identifier 10.1109/TPEL.2023.3326383

applications such as electric vehicles are so important that they cannot be neglected in terms of both performance and the control system health [33]. For this reason, advanced nonlinear control methods should be used in the control of nonlinear systems such as induction motors. In studies in the literature, adaptive control [34], [35], robust control [36], [37], fuzzy logic control [38], [39], [40], MPC [41], [42], [43], neural networks [44], [45] and sliding mode control (SMC) [46], [47], [48], [49] etc. methods have been developed.

The SMC method stands out among the nonlinear control techniques because it has advantages which include being less susceptible to disturbance effects and without requiring model parameters [50], [51]. However, there are several serious drawbacks to conventional SMC, such as the chattering issue brought on by the high switching frequency [52], [53]. Many solutions have been put out to deal with this issue. The SMC method with the disturbance observer is one of the techniques used to stop chattering [54], [55], however it hasn't been able to completely eliminate the issue [56]. Super-twisting SMC method eliminates chattering, although it results in significant overshoots [57]. Although the integral SMC approach [58] and the back-stepping SMC method [59] have partially addressed the chattering issue, these techniques work well when dealing with time-invariant or extremely slow-changing disturbance effects. SMC based on disturbance observers can only reduce chattering to a certain extent [60], [61]. Therefore, the SMC method still needs to be developed [62]. The two parts of the SMC structure are the reaching mode and the sliding mode. The system which is controlled can reaching the slip surface using the reaching mode, however it is very challenging to keep the system there error-free [63]. A chattering problem arises when the system starts to oscillate above the sliding surface. The elimination of the chattering issue is the most crucial aspect of the conventional SMC technique. As a result, it is crucial to create the reaching mode since it directly relates to the chattering problem and has a significant impact on the control system dynamic response [64], [65]. Because of this, certain techniques have been developed on the reaching mode to address the chattering issue as well as boost system performance by rapidly reaching the slip surface. The exponential SMC approach is the first of these techniques. This approach adds the exponential component in addition to the constant term used in the conventional reaching mode, but it still requires a faster approach to the slip surface to reduce chattering [66]. This approach loses convergence as it advances away from the slip surface, although having the benefit of rapid convergence in the regions adjacent to the slip surface [46]. The terminal SMC approach is another developed technique as a solution to the problems of convergence and chattering [32], [67], [68]. In comparison to the conventional SMC and the exponential SMC, it is thus quite successful from the point of both the speed of reaching sliding surface and the chattering problem [32]. However, in this method, the speed of reaching the sliding surface still needs to be increased. Main disadvantages of terminal SMC are the singular problem and low speed of convergence [69]. Although this approach has a rapid convergence advantage in areas near the slip surface, the benefit of convergence diminishes as one advances farther away from the slip surface [46]. As a result, terminal SMC needs to be improved upon and its drawbacks should be minimized.

This article suggests a new adaptive terminal SMC (ATSMC) method for speed management of induction motor with DTC. Flux weakening control with MPC is used to drive the induction motor at high speeds. However, the MPC-based flux weakening control has a significant disadvantage, such as high ripple in the driver system. The purpose of this article is to improve speed control performance of DTC controlled induction motor with MPC-based control. In addition to advancing control performance, the method also aim to reduce chattering. In the suggested ATSMC algorithm both the exponential component and the constant rate term has been developed. An inverse hyperbolic sine function is presented to the constant rate term in the suggested ATSMC approach, which will quicken the system access to the slip surface and lessen chattering. As the dependent variable approaches zero, the inverse hyperbolic sine function approaches zero more quickly. The exponential term has also been added as the upper force in order more to reduce the chattering and improve access to the sliding surface of the control system. Consequently, ATSMC is made possible, which has a quicker dynamic response and less clattering. Moreover, the chattering issue of terminal SMC method and system latency are avoided. Additionally, the suggested advanced speed control significantly reduces the torque and flux oscillations present in the MPC-based flux weakening control. The validity and success of the proposed method has been demonstrated both by simulation and experimental results.

II. Direct Torque Control of Induction Motor

The block scheme of the whole control drive system of the induction motor is given in Fig. 1. Here, the induction motor drive system consists of three main controllers: flux weakening control, speed control and DTC.

A. Induction Motor Dynamic Model

Induction motor consists of two basic components which are rotor and stator windings. Three-phase voltage supplies the windings in stator, and so current flows through the windings. These three-phase currents generate a rotating magnetic field. The rotor conductors experience an increase in voltage in accordance with the induction principle, which causes alternating current to begin flowing through them. The rotor moves as a result of locking the rotor magnetic field into the rotating magnetic field. The stator and rotor dynamic equations can be written as follows:

$$v_{sd} = R_s\, i_{sd} + \frac{d\psi_{sd}}{dt} - \omega_s \psi_{sq} \tag{1}$$

$$v_{sq} = R_s\, i_{sq} + \frac{d\psi_{sq}}{dt} + \omega_s \psi_{sd} \tag{2}$$

$$\psi_{sd} = L_s\, i_{sd} + M i_{rd} \tag{3}$$

$$\psi_{sq} = L_s\, i_{sq} + M i_{rq} \tag{4}$$

$$T_e = p\,(i_{sq}\psi_{sd} - i_{sd}\psi_{sq}) \tag{5}$$

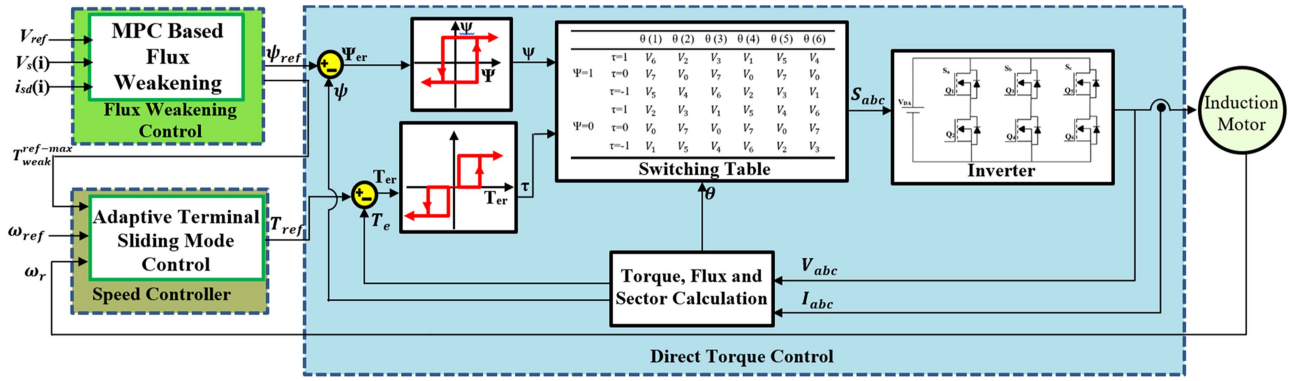

Fig. 1. Block scheme of ATSMC speed control for DTC controlled induction motor drive.

$$\omega_r = \frac{1}{B}\left(J\frac{d\omega_r}{dt} - T_e + T_l\right). \tag{6}$$

In (1)–(6), v_{sd}, v_{sq}, i_{sd}, i_{sq}, i_{rd}, i_{rq}, ψ_{sd}, and ψ_{sq} stand for the d- and q-axis of the stator voltage, stator current, rotor current and stator flux, respectively. R_s, L_s, M, p, J, T_e, T_l, B, and ω_r stand for the stator resistance, stator inductance, mutual inductance, pole pair number, inertia, induced torque, load torque, friction and motor speed, respectively.

The voltage restrictions must be taken into account when applying voltage to the motor. Likewise, stator winding currents must also stay within acceptable bounds. Thus, the following restriction may be applied:

$$i_{sd}^2 + \sigma^2 i_{sq}^2 \le \left(\frac{V_{\max}}{\omega_r L_s}\right)^2. \tag{7}$$

In (7), $\sigma = 1 - \frac{L_m^2}{L_s L_r}$ is the leakage element. Additionally, current limit is written as follows:

$$i_{sd}^2 + i_{sq}^2 \le i_{\max}^2. \tag{8}$$

Depending on the nominal current level of the used inverter and motor, $i_{\max}$ is the highest current value that can be obtained. Stator current is converted from three-axes to two-axes grid for motor control. i_{sd} controls the motor flux, whereas i_{sq} controls the torque.

B. Direct Torque Control

The DTC model used in this article is given in Fig. 1. The induction motor current and voltage are monitored to use this technique. The motor flux, torque, and flux sector are determined using the measured data. The two-level hysteresis controller receives the flux error. Similarly, three-level hysteresis controller is used to manage the torque error. Using the signals obtained from the hysteresis controller and the predicted flux sector, switching signals are generated to apply to induction motor driver.

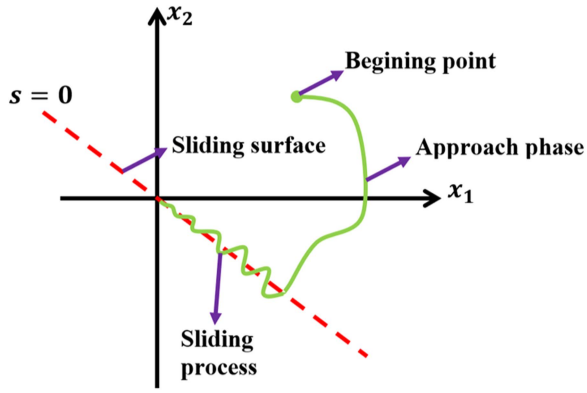

Fig. 2. Sliding surface of the system.

III. Flux Weakening Control

This topic (classic and MPC-based flux weakening control) is covered in detail in the Authors' other previously published paper [26].

IV. Speed Control of Induction Motor

A. Conventional Sliding Mode Control

The sliding mode controller is a type of control with a nonlinear structure. For this reason, its success in the control of nonlinear systems such as induction motors is quite high. Another advantage of this system is that it is less sensitive to system parameters and external disturbances [70]. The aim of the SMC process is to direct the controlled system on the sliding surface and to keep this surface around the equilibrium point. When the slip surface of a second order system given in Fig. 2 is examined, the relationship between the state variables and dynamics of the sliding surface system is clearly seen. In Fig. 2, it is understood that the control structure consists of two parts. The first part is the approach phase from the starting point to the slip surface. The other part is the slip surface where the system moves to the equilibrium point. In order to work this system successfully, two stages are required [70]. These stages are to find the slip surface and design the controller that will direct the system to the slip surface and keep it on this surface.

The relationship between the state variables $\omega_{\text{ref}}(t)$ and $\omega_r(t)$ and the state dynamics in the sliding mode controller design for induction motor speed control is determined as follows:

$$x_1(t) = \omega_{\text{ref}}(t) - \omega_r(t) \tag{9}$$

$$x_2(t) = \dot{x}_1(t). \tag{10}$$

With the determined state dynamics, the slip surface ($s(t)$) of the system can be written as follows [71]:

$$s(t) = x_2(t) + \lambda x_1(t). \tag{11}$$

Here, λ is the slip surface coefficient. To make it easier for the system to reach the sliding surface and reduce chattering, the sliding surface can be rearranged as shown [72]

$$\dot{s}(t) = -\varepsilon \text{sgn}(s(t)) - ks(t). \tag{12}$$

Here, ε and k are switching gain and exponential component coefficient, respectively. ε and k directly affect the controller performance. If these values are chosen large enough, time to reach the slip surface will be shortened and thus speed of the controller will increase [71]. According to the induction motor dynamic equations in (1)–(6), the following equation can be written:

$$\dot{\omega}_r(t) = (T_{\text{ref}} - T_l)/J. \tag{13}$$

Using (9), (11), (12), and (13), the following equation is obtained:

$$\dot{x}_2(t) + \lambda(\dot{\omega}_{\text{ref}}(t) - \dot{\omega}_r(t)) = -\varepsilon \text{sgn}(s(t)) - ks(t). \tag{14}$$

Using (14) the torque reference can be written as follows:

$$T_{\text{ref}} = \frac{J}{\lambda}[\dot{x}_2(t) + \lambda\dot{\omega}_{\text{ref}}(t) + \varepsilon \text{sgn}(s(t)) + ks(t)] + T_l. \tag{15}$$

1) Stability Analysis: The Lyapunov stability function has been chosen so that the system dynamics can be stable. The Lyapunov is as follows:

$$V(t) = \frac{1}{2}s^2(t) > 0 \tag{16}$$

$$\dot{V}(t) = s(t)\dot{s}(t) \le 0. \tag{17}$$

Using (11), (12) and (17) the following equation can be obtained:

$$\dot{V}(t) = -|s(t)|\varepsilon - ks^2(t) \le 0. \tag{18}$$

In (18), if k>0 and ε>0 are selected, the stability condition is fulfilled.

B. Adaptive Terminal Sliding Mode Control

In the SMC method, ε and k should be chosen large enough for the control process to be fast, but in this case, the chattering problem will arise. Therefore, both the dynamic response speed and the chattering problem should be considered while designing the controller. In this article, the adaptive terminal slip surface access mode given below is suggested instead of the slip surface access mode given in (12) in order to both accelerate the dynamic response of the controller and prevent the chattering problem

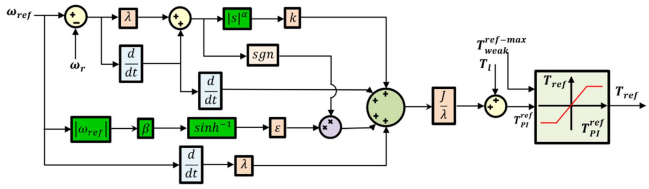

Fig. 3. Suggested adaptive terminal sliding mode controller block schema.

$$\dot{s}(t) = -\varepsilon \text{sinh}^{-1}(\beta|x_1(t)|)\text{sgn}(s(t)) - k|s(t)|^{\alpha}\ \beta > 0, \alpha > 0. \tag{19}$$

Although choosing ε and k large enough in conventional access mode accelerates the dynamic response of the controller, both the speed is not sufficient. The success of the SMC method directly depends on the reaching law which determines the speed and time at which the system reaches the sliding surface. The speed of reaching the slip surface directly affects the performance of the controller. Therefore, if the reaching law is arranged so that the controller can reach the sliding surface faster, both the performance of the controller will be increased and the chattering problem will be reduced. Therefore, in this article, a new ATSMC has been proposed to increase the speed of reaching the slip surface. First, an inverse hyperbolic sine function is adding to the constant rate term, which will accelerate the system access to the slip surface and lessen chattering. As the dependent variable in inverse hyperbolic sine function approaches zero, the function approaches zero more quickly. In addition, the exponential term has also been added as the upper force to further increase the speed of the law of reaching. therefore, fast reaching law ensure low chattering and good dynamics reaction. Therefore, in the suggested ATSMC as seen in (19), two new terms have been added, different from the conventional SMC. One of the added terms is $\text{sinh}^{-1}(\beta|x_1(t)|)$. The value of the inverse hyperbolic sine function will quickly approach zero as the defined variable ($x_1(t)$) approaches zero. This feature provides a significant advantage to ATSMC for controlling the speed. It will also reduce chattering. The other term added is the power term added to the exponential term of the reaching mode. With this exponential force, both the response speed of the controller will be increased and the chattering will be minimized.

Using the proposed slip access mode and (9), (11), (12), and (13) the new torque reference can be written as follows. A detailed version of the proposed method is given in Fig. 3.

$$T_{\text{ref}} = \frac{J}{\lambda}[\dot{x}_2(t) + \lambda\dot{\omega}_{\text{ref}}(t) + \varepsilon \text{sinh}^{-1}(\beta|x_1(t)|)\text{sgn}(s(t)) + k|s(t)|^{\alpha}] + T_l. \tag{20}$$

V. Simulation Results

The proposed ATSMC method simulation is carried out in MATLAB platform. For this purpose, the control system block diagram given in Fig. 1 is designed with MATLAB. The induction motor is modeled using (1)–(6). Table I gives specifications of the used motor in both experimental and simulation study. In simulation, the speed reference depicted in Fig. 4 has applied.

TABLE I
PARAMETERS OF INDUCTION MOTOR

Parameter	Value
P (kW)	1.1
Voltage (V)	380
Speed (rpm)	1430
R_s (Ω)	7.7
L_s (H)	0.0617
R_r (Ω)	15.704
L_r (H)	0.0617
R_c (Ω)	882.42
L_m (H)	0.04963
p	2
J (kg m^2)	0.00689
B (N·m-s/rad)	0.00689

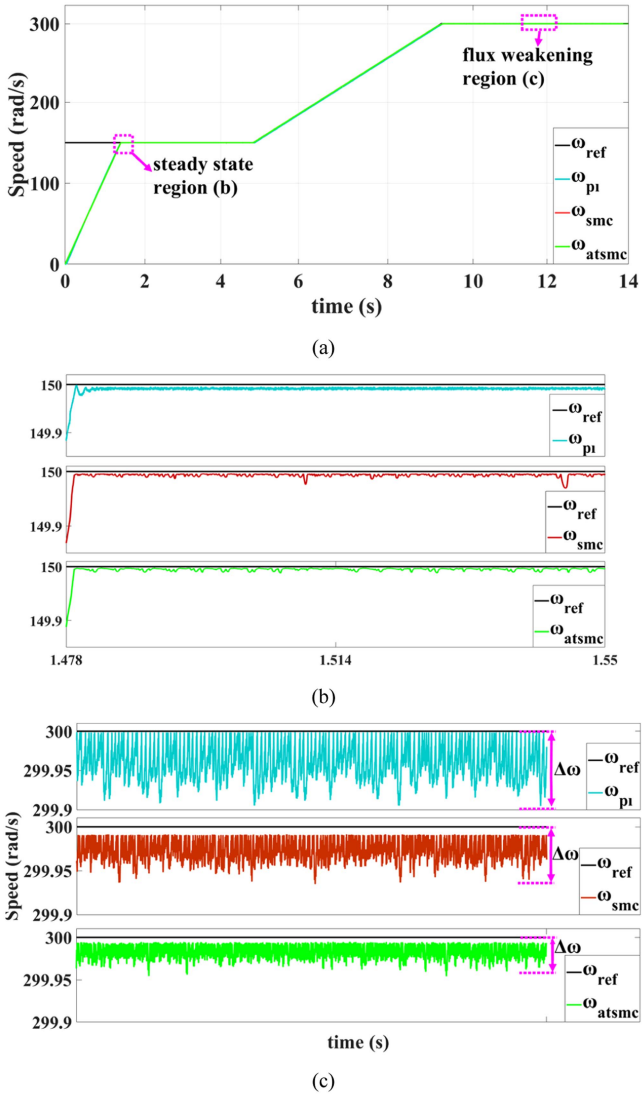

Fig. 4. Simulation results of induction motor speed. (a) Whole speed. (b) Nominal speed. (c) Flux weakening region speed.

In Fig. 4, speed plots for the PI control, SMC, and ATSMC speed control methods DTC drived induction motor drive are demonstrated as a result of the simulation study.

In Fig. 4, the performance of the speed control methods (PI, SMC, and ATSMC) both in the nominal speed region and in the flux weakening region is seen. As seen in Fig. 4(b), the amount of overshoot and ripple for nominal speed is higher in the PI control method. In addition, ompared with SMC and ATSMC, the settle time to the nominal value of the motor speed is also long. As can be seen in Fig. 4(b), the stated problems have been quite resolved with SMC, but the chattering problem is seen in the graphics. With the proposed ATSMC, both the problems in the PI control have been eliminated and the chattering problem has been reduced. As seen in Fig. 4(c), the ripple of speed for PI control is high for flux weakening region because of MPC-based flux control. Even as SMC minimizes this ripple, it is not enough. With the proposed ATSMC, the ripple in speed is considerably reduced.

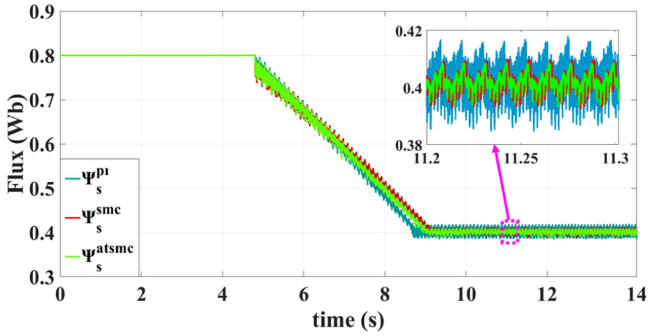

Fig. 5. Flux variation in simulation.

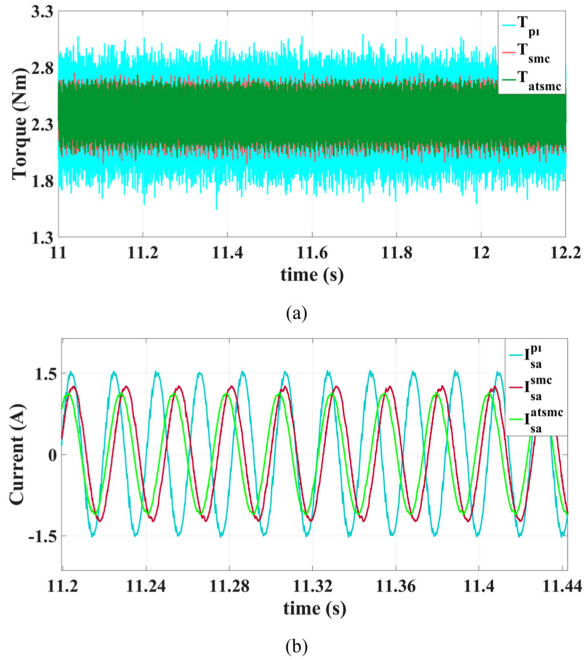

Fig. 6. Simulation results for flux weakening region. (a) Torque. (b) Current.

In addition to the speed, motor flux, current, and torque graphs show that the proposed ATSMC is effective in controlling the motor. Figs. 5 and 6 make it evident that the fundamental drawback of flux weakening control with MPC, excessive flux and torque ripple, is present. The expected reduction in flux and torque ripple has been achieved with the suggested ATSMC. The

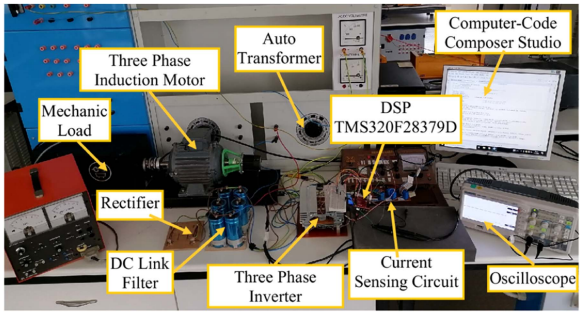

Fig. 7. Experimental platform of induction motor drive.

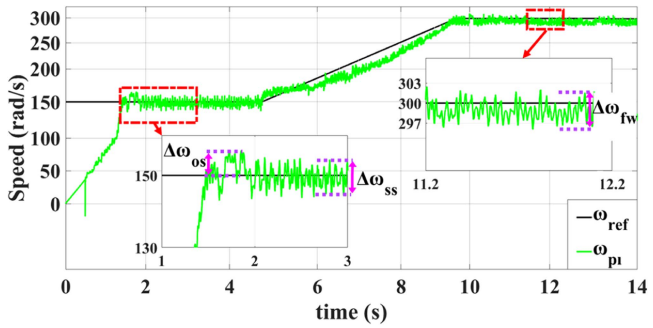

Fig. 8. Experimental results of induction motor speed for PI control.

amount of ripple in flux for PI, SMC and ATSMC is 0.0362, 0.0278, and 0.0274, respectively. Additionally, the amount of ripple in torque for PI, SMC and ATSMC is 0.911, 0.513, and 0.215, respectively. As can be observed from the current plot, the lowering of the current level further demonstrates the validity of the suggested strategy. Besides, total harmonic distorsion (THD) of stator phase a for PI, SMC, and ATSMC is 2.38, 1.797, and 1.75, respectively.

The suggested adaptive terminal sliding mode controller block schema is given in Fig. 3, accompanied by the above equations and explanations.

VI. Experimental Results

To show success of the suggested ATSMC, the platform given in the Fig. 7 has been established, in the flux weakening region of the induction motor. Flux weakening control of DTC controlled induction motor has been carried out with MPC. Table I gives the specifications of the induction motor that has been used in the control platform. DSP TMS320F28379D dual-core micro-controller of Texas Instrument has been used for DTC, MPC-based flux weakening and speed control methods (PI, SMC, and ATSMC) used for induction motor control. All circuits in the setup (inverter, dc bus filter, MOSFET driver, dead-time circuit, current sensing circuit, etc.) have been designed and implemented in the laboratory.

The setup shown in Fig. 7 has been designed in order to assess the effectiveness of speed control techniques in the flux weakening region using MPC-based control. The performance of the induction motor for PI control in the rated speed and flux weakening region is shown in Fig. 8. The motor flux plot during

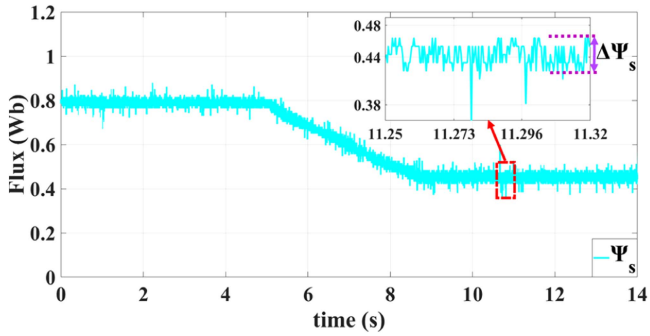

Fig. 9. Flux variation for PI control in experimental.

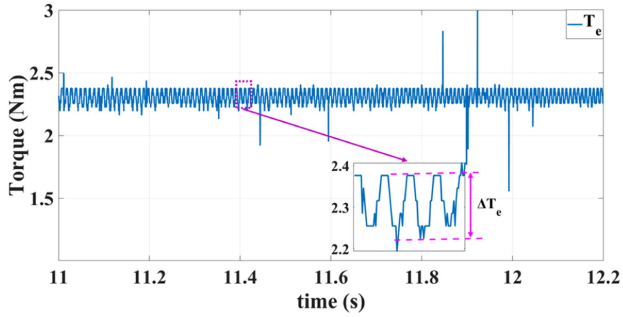

(a)

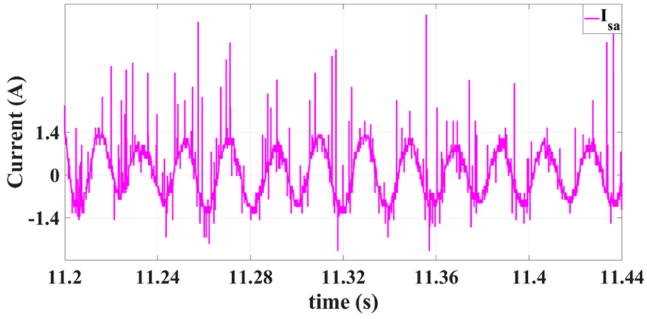

(b)

Fig. 10. Experimental result in flux weakening region for PI control. (a) Torque. (b) Current.

TABLE II
Speed Results for Speed Control Methods

Parameter	PI	SMC	ATSMC
$\Delta\omega_{os}$	6.23	0	0
$\Delta\omega_{ss}$	8.31	6.24	5.65
t_s	1.91	1.56	1.52
$\Delta\omega_{fw}$	5.44	4.05	2.62

the test process is shown in Fig. 9. The torque and current plots obtained in the flux weakening region are shown in Fig. 10. Here, especially in the current measurement results, there is noise due to the sensors and circuitry used. The numerical data for specified ripple in speed, steady state settling time and overshoot are given in Table II. Numerical data for the specified ripple in torque and flux and THD value for stator current are given in Table III.

Fig. 11 displays the induction motor performance for SMC control in the rated speed and flux weakening range. The motor

TABLE III
PERFORMANCE COMPARISON FOR SPEED CONTROL METHODS

Parameter	PI	SMC	ATSMC
THD_{isa}	8.7172	6.84	6.17
$\Delta\Psi_s$	0.0603	0. 0513	0.0267
ΔT_e	0.264	0.237	0.215

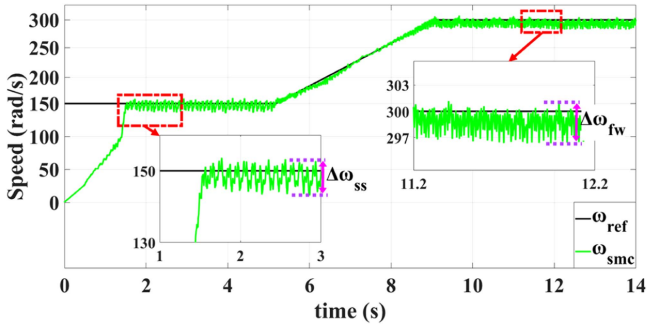

Fig. 11. Experimental results of induction motor speed for SMC.

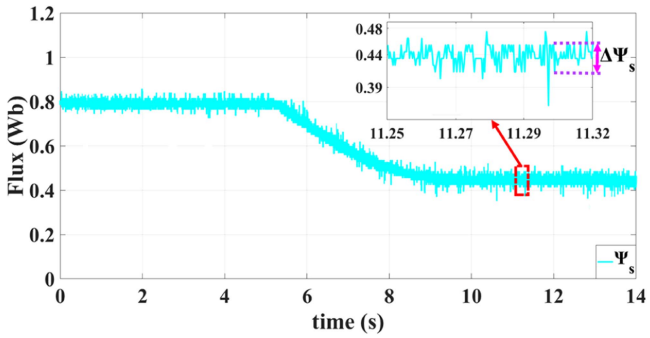

Fig. 12. Flux variation for SMC in experimental.

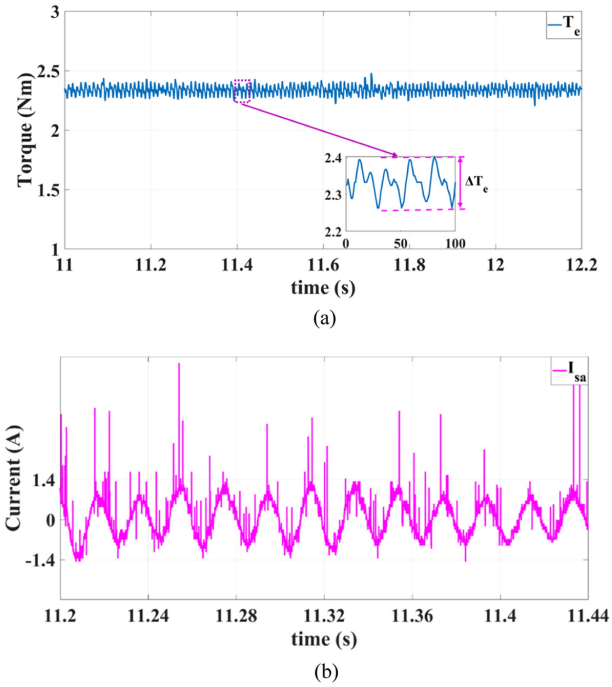

Fig. 13. Experimental result in flux weakening for SMC. (a) Torque. (b) Current.

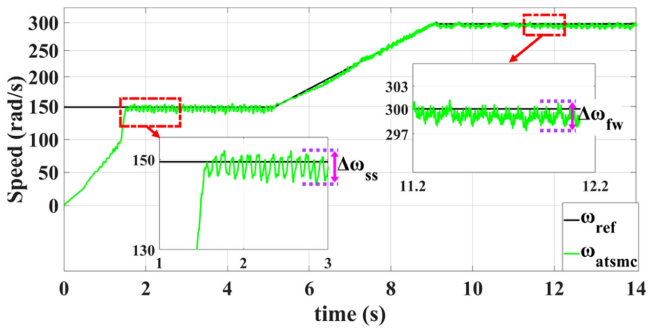

Fig. 14. Experimental results of induction motor speed for ATSMC. (a) Whole speed and nominal speed. (b) Flux weakening region speed.

flux plot during the test process is seen in Fig. 12. Fig. 13 displays the torque and current plots acquired in the flux weakening region. The numerical data for the specified ripple in speed, steady state settling time and overshoot are given in Table II. The numerical data for specified ripple in torque and flux and THD value for stator current are given in Table III.

The performance of the induction motor for ATSMC control in the rated speed and flux weakening region is shown in Fig. 14. The motor flux plot during the test process is shown in Fig. 15. The torque and current plots obtained in flux weakening region are shown in Fig. 16. Table II provides the numeric data for specified overshoot, steady state settling time, and speed ripple. The numerical data for the specified ripple in torque and flux and THD value for stator current are given in Table III.

The numerical data for the specified ripple in speed, steady state settling time and overshoot are given in Table II for simulation and experimental study. When Table II is examined, the overshoot values ($\Delta\omega_{os}$) as a result of the PI control for both simulation and experimental study is completely damped in the SMC and ATSMC methods. At the same time, the steady-state settling time (t_s) of the motor speed has been boosted with SMC. With the proposed ATSMC method, the steady state settling time is further reduced. When the data in Table II is examined, the amount of ripple in speed for both the nominal speed and the flux weakening region ($\Delta\omega_{ss}$ and $\Delta\omega_{fw}$) is reduced by SMC. With the proposed ATSMC, the ripple, especially in the flux weakening region, has been considerably reduced compared to both PI and SMC methods as a result of both simulation and experimental study. When both the data in the tables and the speed plots in Figs. 8, 11, and 14 are examined, better convergence and less chattering are obtained with the new terms added in the proposed ATSMC compared to SMC.

Parameter uncertainties may have an impact on the torque calculation and algorithm output value at the time of the parameter variation. However, the system can still monitor the reference of the control signal and meet the need for system durability since it possesses robust sliding-mode structural properties. When Figs. 8, 11, and 14 are examined, the speed reference is followed with higher accuracy, especially with ATSMC, despite the parameter uncertainties. The data in Table II for both the

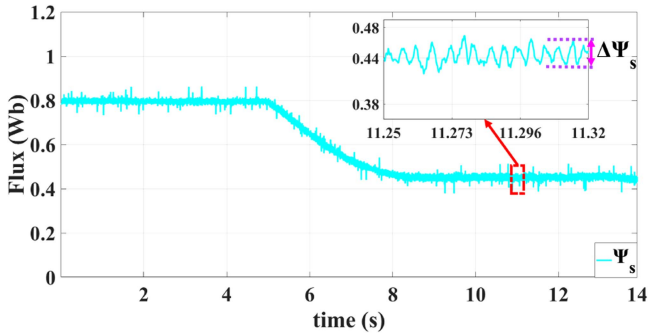

Fig. 15. Flux variation for ATSMC in experimental.

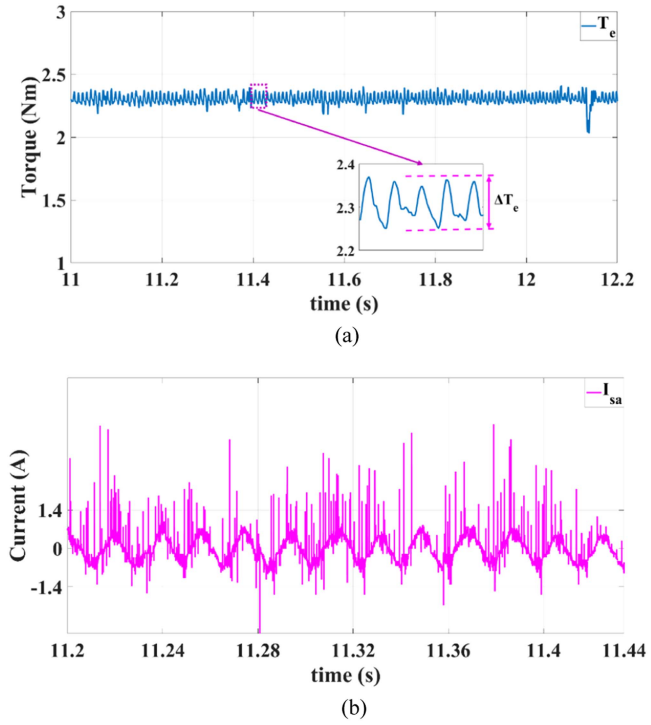

Fig. 16. Experimental result in flux weakening for ATSMC. (a) Torque. (b) Current.

rated speed and the flux weakening region support this. Parameter changes affect the calculation of reference values such as torque in the control algorithm. When Figs. 10, 13, and 16 are examined, the performance is lower with PI control and higher with ATSMC control due to parameter changes. The findings give significant support for the precision ATSMC control of induction motor because they demonstrate that ATSMC control still exhibits high resilience in the presence of parameter mismatch.

To more clearly demonstrate how well the suggested ATSMC method performs, the numerical data for the specified ripple in torque and flux and THD value for stator current are given in Table III. The stator current THD value (THD_{isa}) is significantly decreased using SMC and ATSMC, as given in Table III. Additionally, It is noticed that ripple in flux ($\Delta\Psi_s$) and torque (ΔT_e) is high for MPC-based flux weakening control for PI control. It has been demonstrated through simulation and experimental study that SMC reduces the level of flux and torque ripple. When compared to PI and SMC approaches, the suggested ATSMC significantly reduces ripple in both flux and torque. Analyzing Tables II and III, and graphs reveals that, although the problems of the PI control application have been resolved using with SMC, a chattering problem has occurred with the conventional SMC. It is clear that one inherited problem with the SMC controller—the chattering phenomenon—has some negative effects on the system's performance. As can be seen from both the tables and Figs. 12, 13, 15, and 16, chattering has been significantly reduced with the proposed ATSMC.

VII. Conclusion

In this article, a new ATSMC method is suggested for speed control of DTC controlled induction motor. The suggested approach has been tested by simulation and experimental results. The induction motor has been operated at high speeds using flux weakening control based on the MPC. In this article, a new ATSMC has been suggested and used as a way to get rid of issues such ripples in motor output parameters caused on by MPC-based flux weakening control while also improving speed control performance. According to both simulation and experimental study results, besides the improvement of motor control performance with conventional SMC, ripples in motor speed, flux and torque have been reduced, but the chattering problem occurred. The exponential term and constant rate term of conventional SMC method are both modified and a new ATSMC method has been suggested to both increase the speed control efficiency and eliminate the chattering problem and for a quick convergence. The suggested ATSMC has produced less speed error, overshoot, and ripple in both the nominal speed and flux weakening region, as well as shorter steady state settling time, according to the speed plots produced as a consequence of the study and the data in the tables. In addition to the improvement in speed, the motor current THD value decreased, ripple in flux and torque, which are the most significant drawbacks of the flux weakening control with MPC based flux weakening control, are significantly minimized.

References

[1] J.-R. Riba, C. López-Torres, L. Romeral, and A. Garcia, "Rare-earth-free propulsion motors for electric vehicles: A technology review," *Renew. Sustain. Energy Rev.*, vol. 57, pp. 367–379, 2016.

[2] C. G. Dias and L. C. Silva, "Induction motor speed estimation based on airgap flux measurement using Hilbert transform and fast Fourier transform," *IEEE Sensors J.*, vol. 22, no. 13, pp. 12690–12699, Jul. 2022.

[3] S. A. Saleh, E. Ozkop, M. Ş. Ayas, K. M. Muttaqi, and B. Nahid-Mobarakeh, "Survivability-based protection for electric motor drive systems-Part I: 3ϕ induction motor drives," *IEEE Trans. Ind. Appl.*, vol. 58, no. 2, pp. 1797–1808, Mar./Apr. 2022.

[4] M. S. A. M. Omara and A. A. Z. Diab, "Cascaded fuzzy logic based direct torque control of interior permanent magnet synchronous motor for variable speed electric drive systems," in *Proc. 25th Int. Workshop Elect. Drives, Optim. Control Elect. Drives*, 2018, doi: 10.1109/IWED.2018.8321386.

[5] M. S. Arifin, M. N. Uddin, and W. Wang, "Neuro-fuzzy adaptive direct torque and flux control of a grid-connected DFIG-WECS with improved dynamic performance," *IEEE Trans. Ind. Appl.*, early access, Aug. 7, 2023, doi: 10.1109/TIA.2023.3302844.

[6] I. Takahashi and T. Noguchi, "A new quick-response and high-efficiency control strategy of an induction motor," *IEEE Trans. Ind. Appl.*, vol. IA-22, no. 5, pp. 820–827, Sep. 1986.

[7] K.-K. Shyu, J.-K. Lin, V.-T. Pham, M.-J. Yang, and T.-W. Wang, "Global minimum torque ripple design for direct torque control of induction motor drives," *IEEE Trans. Ind. Electron.*, vol. 57, no. 9, pp. 3148–3156, Sep. 2009.

[8] H. Aygun and M. Aktas, "LMC-based DTC for efficiency improvement of IM drives and their electric vehicle applications," *J. Power Electron.*, vol. 20, pp. 1232–1242, 2020.

[9] J. Su, R. Gao, and I. Husain, "Model predictive control based field-weakening strategy for traction EV used induction motor," *IEEE Trans. Ind. Appl.*, vol. 54, no. 3, pp. 2295–2305, May/Jun. 2018.

[10] M. Farasat, A. M. Trzynadlowski, and M. S. Fadali, "Efficiency improved sensorless control scheme for electric vehicle induction motors," *Inst. Eng. Technol. Elect. Syst. Transp.*, vol. 4, no. 4, pp. 122–131, 2014.

[11] H. Liu, Z. Q. Zhu, E. Mohamed, Y. Fu, and X. Qi, "Flux-weakening control of nonsalient pole PMSM having large winding inductance, accounting for resistive voltage drop and inverter nonlinearities," *IEEE Trans. Power Electron.*, vol. 27, no. 2, pp. 942–952, Feb. 2012.

[12] Z. Yin, C. Zhao, Y.-R. Zhong, and J. Liu, "Research on robust performance of speed-sensorless vector control for the induction motor using an interfacing multiple-model extended Kalman filter," *IEEE Trans. Power Electron.*, vol. 29, no. 6, pp. 3011–3019, Jun. 2014.

[13] M.-H. Shin, D.-S. Hyun, and S.-B. Cho, "Maximum torque control of stator-flux-oriented induction machine drive in the field-weakening region," *IEEE Trans. Ind. Appl.*, vol. 38, no. 1, pp. 117–122, Jan./Feb. 2002.

[14] M.-H. Shin and D.-S. Hyun, "Speed sensorless stator flux-oriented control of induction machine in the field weakening region," *IEEE Trans. Power Electron.*, vol. 18, no. 2, pp. 580–586, Mar. 2003.

[15] L. Harnefors, K. Pietilainen, and L. Gertmar, "Torque-maximizing field-weakening control: Design, analysis, and parameter selection," *IEEE Trans. Ind. Electron.*, vol. 48, no. 1, pp. 161–168, Feb. 2001.

[16] M. Mengoni, L. Zarri, A. Tani, G. Serra, and D. Casadei, "Stator flux vector control of induction motor drive in the field weakening region," *IEEE Trans. Power Electron.*, vol. 23, no. 2, pp. 941–949, Mar. 2008.

[17] M. Mengoni, L. Zarri, A. Tani, G. Serra, and D. Casadei, "A comparison of four robust control schemes for field-weakening operation of induction motors," *IEEE Trans. Power Electron.*, vol. 27, no. 1, pp. 307–320, Jan. 2012.

[18] P.-Y. Lin and Y.-S. Lai, "Novel voltage trajectory control for field-weakening operation of induction motor drives," *IEEE Trans. Ind. Appl.*, vol. 47, no. 1, pp. 122–127, Jan./Feb. 2010.

[19] S.-H. Kim and S.-K. Sul, "Maximum torque control of an induction machine in the field weakening region," *IEEE Trans. Ind. Appl.*, vol. 31, no. 4, pp. 787–794, Jul./Aug. 1995.

[20] G. Gallegos-Lopez, F. S. Gunawan, and J. E. Walters, "Current control of induction machines in the field-weakened region," *IEEE Trans. Ind. Appl.*, vol. 43, no. 4, pp. 981–989, Jul./Aug. 2007.

[21] Y. Wang, Y. Shi, Y. Xu, and R. D. Lorenz, "A comparative overview of indirect field oriented control (IFOC) and deadbeat-direct torque and flux control (DB-DTFC) for AC motor drives," *Chin. J. Elect. Eng.*, vol. 1, no. 1, pp. 9–20, 2015.

[22] S. E. Rezgui, A. Mehdi, S. Legrioui, H. Meddouce, A. M. Boulahia, and H. Benalla, "IRFOC vs DTC performance comparison analysis," in *Proc. 3rd Int. Conf. Elect. Power Energy Convers. Syst.*, 2013, pp. 1–6.

[23] C. Alfaro, R. Guzman, L. G. de Vicuña, J. Miret, and M. Castilla, "Dual-loop continuous control set model-predictive control for a three-phase unity power factor rectifier," *IEEE Trans. Power Electron.*, vol. 37, no. 2, pp. 1447–1460, Feb. 2022.

[24] M. Preindl, "Robust control invariant sets and Lyapunov-based MPC for IPM synchronous motor drives," *IEEE Trans. Ind. Electron.*, vol. 63, no. 6, pp. 3925–3933, Jun. 2016.

[25] C. Bai, Z. Yin, Y. Zhang, and J. Liu, "Robust predictive control for linear permanent magnet synchronous motor drives based on an augmented internal model disturbance observer," *IEEE Trans. Ind. Electron.*, vol. 69, no. 10, pp. 9771–9782, Oct. 2022.

[26] B. Çavuş and M. Aktaş, "MPC-based flux weakening control for induction motor drive with DTC for electric vehicles," *IEEE Trans. Power Electron.*, vol. 38, no. 4, pp. 4430–4439, Apr. 2023, doi: 10.1109/TPEL.2022.3230547.

[27] S. Rubino, R. Bojoi, S. A. Odhano, and P. Zanchetta, "Model predictive direct flux vector control of multi-three-phase induction motor drives," *IEEE Trans. Ind. Appl.*, vol. 54, no. 5, pp. 4394–4404, Sep./Oct. 2018.

[28] D. Su, C. Zhang, and Y. Dong, "An improved continuous-time model predictive control of permanent magnetic synchronous motors for a wide-speed range," *Energies*, vol. 10, no. 12, 2017, Art. no. 2051.

[29] N. Chen, Z. Zheng, J. Zhou, Y. Li, and K. Wang, "A novel MPC flux weakening method for induction motor applied in electric wheel," in *Proc. Int. Conf. Elect. Mach. Syst.*, 2013, pp. 113–118.

[30] Z.-H. Liu, J. Nie, H.-L. Wei, L. Chen, X.-H. Li, and H.-Q. Zhang, "A newly designed VSC-based current regulator for sensorless control of PMSM considering VSI nonlinearity," *IEEE J. Emerg. Sel. Topics Power Electron.*, vol. 9, no. 4, pp. 4420–4431, Aug. 2021.

[31] A. Rajeev VK and V. Prasad, "Online adaptive gain for passivity based control for sensorless BLDC motor coupled with DC motor for EV application," *IEEE Trans. Power Electron.*, vol. 38, no. 11, pp. 13625–13634, Nov. 2023.

[32] A. K. Junejo, W. Xu, C. Mu, M. M. Ismail, and Y. Liu, "Adaptive speed control of PMSM drive system based a new sliding-mode reaching law," *IEEE Trans. Power Electron.*, vol. 35, no. 11, pp. 12110–12121, Nov. 2020.

[33] S. R. Mahapatro, B. Subudhi, and S. Ghosh, "Design of a robust optimal decentralized PI controller based on nonlinear constraint optimization for level regulation: An experimental study," *IEEE/CAA J. Automatica Sinica*, vol. 7, no. 1, pp. 187–199, Jan. 2019.

[34] J. Talla, V. Q. Leu, V. Šmídl, and Z. Peroutka, "Adaptive speed control of induction motor drive with inaccurate model," *IEEE Trans. Ind. Electron.*, vol. 65, no. 11, pp. 8532–8542, Nov. 2018.

[35] W. Xu, Y. Jiang, C. Mu, and F. Blaabjerg, "Improved nonlinear flux observer-based second-order SOIFO for PMSM sensorless control," *IEEE Trans. Power Electron.*, vol. 34, no. 1, pp. 565–579, Jan. 2019.

[36] B. Wang, C. Luo, Y. Yu, G. Wang, and D. Xu, "Antidisturbance speed control for induction machine drives using high-order fast terminal sliding-mode load torque observer," *IEEE Trans. Power Electron.*, vol. 33, no. 9, pp. 7927–7937, Sep. 2018.

[37] F. Mwasilu and J.-W. Jung, "Enhanced fault-tolerant control of interior PMSMs based on an adaptive EKF for EV traction applications," *IEEE Trans. Power Electron.*, vol. 31, no. 8, pp. 5746–5758, Aug. 2016.

[38] G. Du, W. Xu, J. Zhu, and N. Huang, "Effects of design parameters on the multiphysics performance of high-speed permanent magnet machines," *IEEE Trans. Ind. Electron.*, vol. 67, no. 5, pp. 3472–3483, May 2020.

[39] P. Mani, R. Rajan, L. Shanmugam, and Y. H. Joo, "Adaptive fractional fuzzy integral sliding mode control for PMSM model," *IEEE Trans. Fuzzy Syst.*, vol. 27, no. 8, pp. 1674–1686, Aug. 2019.

[40] D. Xu, J. Huang, X. Su, and P. Shi, "Adaptive command-filtered fuzzy backstepping control for linear induction motor with unknown end effect," *Inf. Sci.*, vol. 477, pp. 118–131, 2019.

[41] A. Ammar, A. Benakcha, and A. Bourek, "Adaptive MRAC-based direct torque control with SVM for sensorless induction motor using adaptive observer," *Int. J. Adv. Manuf. Technol.*, vol. 91, no. 5, pp. 1631–1641, 2017.

[42] H. Du, X. Chen, G. Wen, X. Yu, and J. Lü, "Discrete-time fast terminal sliding mode control for permanent magnet linear motor," *IEEE Trans. Ind. Electron.*, vol. 65, no. 12, pp. 9916–9927, Dec. 2018.

[43] W. Xu, J. Zou, and C. Mu, "Improved model predictive current control strategy-based rotor flux for linear induction machines," *IEEE Trans. Appl. Supercond.*, vol. 26, no. 7, Oct. 2016, Art. no. 0608605.

[44] J. Yu, P. Shi, W. Dong, B. Chen, and C. Lin, "Neural network-based adaptive dynamic surface control for permanent magnet synchronous motors," *IEEE Trans. Neural Netw. Learn. Syst.*, vol. 26, no. 3, pp. 640–645, Mar. 2015.

[45] H. Sathishkumar and S. Parthasarathy, "A novel neural network intelligent controller for vector controlled induction motor drive," *Energy Procedia*, vol. 138, pp. 692–697, 2017.

[46] A. K. Junejo et al., "Novel fast terminal reaching law based composite speed control of PMSM drive system," *IEEE Access*, vol. 10, pp. 82202–82213, 2022.

[47] J. Liu, H. Li, and Y. Deng, "Torque ripple minimization of PMSM based on robust ILC via adaptive sliding mode control," *IEEE Trans. Power Electron.*, vol. 33, no. 4, pp. 3655–3671, Apr. 2018.

[48] Z. Yin, L. Gong, C. Du, J. Liu, and Y. Zhong, "Integrated position and speed loops under sliding-mode control optimized by differential evolution algorithm for PMSM drives," *IEEE Trans. Power Electron.*, vol. 34, no. 9, pp. 8994–9005, Sep. 2019.

[49] Y. Jiang, W. Xu, C. Mu, and Y. Liu, "Improved deadbeat predictive current control combined sliding mode strategy for PMSM drive system," *IEEE Trans. Veh. Technol.*, vol. 67, no. 1, pp. 251–263, Jan. 2018.

[50] J. Mao, H. Li, Y. Zhou, L. Yang, and J. Huang, "Direct speed composite control of SPMSM drive system," *IEEE J. Emerg. Sel. Topics Power Electron.*, vol. 11, no. 5, pp. 5120–5130, Oct. 2023.
[51] W. Zhu, X. Li, X. Cao, Y. Li, and K. Zhou, "An improved modulation strategy without current zero-crossing distortion and control method for Vienna rectifier," *IEEE Trans. Power Electron.*, early access, Aug. 4, 2023, doi: 10.1109/TPEL.2023.3302130.
[52] B.-C. Zheng and J. H. Park, "Sliding mode control design for linear systems subject to quantization parameter mismatch," *J. Franklin Inst.*, vol. 353, no. 1, pp. 37–53, 2016.
[53] A. Argha, L. Li, S. W. Su, and H. Nguyen, "On LMI-based sliding mode control for uncertain discrete-time systems," *J. Franklin Inst.*, vol. 353, no. 15, pp. 3857–3875, 2016.
[54] W. Kim, D. Shin, D. Won, and C. C. Chung, "Disturbance-observer-based position tracking controller in the presence of biased sinusoidal disturbance for electrohydraulic actuators," *IEEE Trans. Control Syst. Technol.*, vol. 21, no. 6, pp. 2290–2298, Nov. 2013.
[55] Z. Li, F. Wang, D. Ke, J. Li, and W. Zhang, "Robust continuous model predictive speed and current control for PMSM with adaptive integral sliding-mode approach," *IEEE Trans. Power Electron.*, vol. 36, no. 12, pp. 14398–14408, Dec. 2021.
[56] W. Xu, A. K. Junejo, Y. Liu, M. G. Hussien, and J. Zhu, "An efficient antidisturbance sliding-mode speed control method for PMSM drive systems," *IEEE Trans. Power Electron.*, vol. 36, no. 6, pp. 6879–6891, Jun. 2021.
[57] S. Ouchen, M. Benbouzid, F. Blaabjerg, A. Betka, and H. Steinhart, "Direct power control of shunt active power filter using space vector modulation based on supertwisting sliding mode control," *IEEE J. Emerg. Sel. Topics Power Electron.*, vol. 9, no. 3, pp. 3243–3253, Jun. 2021.
[58] Z. Kardous and N. B. Braiek, "Stabilizing multimodel sliding mode control for homogeneous TS-bilinear systems," *J. Franklin Inst.*, vol. 352, no. 1, pp. 177–188, 2015.
[59] C. Mu, W. Xu, and C. Sun, "On switching manifold design for terminal sliding mode control," *J. Franklin Inst.*, vol. 353, no. 7, pp. 1553–1572, 2016.
[60] J. Knight, S. Shirsavar, and W. Holderbaum, "An improved reliability Cuk based solar inverter with sliding mode control," *IEEE Trans. Power Electron.*, vol. 21, no. 4, pp. 1107–1115, Jul. 2006.
[61] J. Van Gorp, M. Defoort, K. C. Veluvolu, and M. Djemai, "Hybrid sliding mode observer for switched linear systems with unknown inputs," *J. Franklin Inst.*, vol. 351, no. 7, pp. 3987–4008, 2014.
[62] M. Zhou, S. Cheng, Y. Feng, W. Xu, L. Wang, and W. Cai, "Full-order terminal sliding-mode-based sensorless control of induction motor with gain adaptation," *IEEE J. Emerg. Sel. Topics Power Electron.*, vol. 10, no. 2, pp. 1978–1991, Apr. 2022.
[63] R.-M. Jan, C.-S. Tseng, and R.-J. Liu, "Robust PID control design for permanent magnet synchronous motor: A genetic approach," *Elect. Power Syst. Res.*, vol. 78, no. 7, pp. 1161–1168, 2008.
[64] S. Lin, Y. Cai, B. Yang, and W. Zhang, "Electrical line-shafting control for motor speed synchronisation using sliding mode controller and disturbance observer," *Inst. Eng. Technol. Control Theory Appl.*, vol. 11, no. 2, pp. 205–212, 2017.
[65] H. Ma and Y. Li, "A novel dead zone reaching law of discrete-time sliding mode control with disturbance compensation," *IEEE Trans. Ind. Electron.*, vol. 67, no. 6, pp. 4815–4825, Jun. 2020.
[66] W. Gao and J. C. Hung, "Variable structure control of nonlinear systems: A new approach," *IEEE Trans. Ind. Electron.*, vol. 40, no. 1, pp. 45–55, Feb. 1993.
[67] H. Wang et al., "Continuous fast nonsingular terminal sliding mode control of automotive electronic throttle systems using finite-time exact observer," *IEEE Trans. Ind. Electron.*, vol. 65, no. 9, pp. 7160–7172, Sep. 2018.
[68] Y. Feng, M. Zhou, F. Han, and X. Yu, "Speed control of induction motor servo drives using terminal sliding-mode controller," *Adv. Variable Struct. Syst. Sliding Mode Control—Theory Appl.*, vol. 115, pp. 341–356, 2018.
[69] L. Yang and J. Yang, "Nonsingular fast terminal sliding-mode control for nonlinear dynamical systems," *Int. J. Robust Nonlinear Control*, vol. 21, no. 16, pp. 1865–1879, 2011.
[70] M. Aktas, K. Awaili, M. Ehsani, and A. Arisoy, "Direct torque control versus indirect field-oriented control of induction motors for electric vehicle applications," *Eng. Sci. Technol., Int. J.*, vol. 23, no. 5, pp. 1134–1143, 2020.
[71] Y. Zhang, Z. Yin, W. Li, J. Liu, and Y. Zhang, "Adaptive sliding-mode-based speed control in finite control set model predictive torque control for induction motors," *IEEE Trans. Power Electron.*, vol. 36, no. 7, pp. 8076–8087, Jul. 2021.
[72] W. Gao, Y. Wang, and A. Homaifa, "Discrete-time variable structure control systems," *IEEE Trans. Ind. Electron.*, vol. 42, no. 2, pp. 117–122, Apr. 1995.

Barış Çavuş received the B.Sc. degree in electrical and electronics engineering from Karadeniz Technical University, Trabzon, Türkiye, in 2015, and the M.Sc. degree in electrical and electronics engineering in 2019 from Ondokuz Mayis University, Samsun, Türkiye, where he is currently working toward the Ph.D. degree.

His research interests include ac motor drives and control, power electronics, and electric vehicles.

Mustafa Aktaş received the B.Sc., M.Sc., and Ph.D. degrees in electrical and electronics engineering from Karadeniz Technical University, Trabzon, Türkiye, in 1992, 1998, and 2006, respectively.

Between 2010 and 2011, he was a Postdoctoral Researcher in electrical and computer engineering with Texas A&M University, College Station, TX, USA. He is currently a Professor with the Department of Electrical and Electronics Engineering, Ondokuz Mayis University, Samsun, Türkiye. His research interests include ac motor drives and control, and electric and hybrid electric vehicles.